

Focalized Brain Transcranial Magnetic Stimulation with the Utilization of a Field Shaper and a Crescent Ferromagnetic Core

Xiao Fang^{1, *}, Wei Liu¹, Yaoyao Luo¹, Chang Liu², and Zhou He²

Abstract—Transcranial magnetic stimulation (TMS) has been widely used in the treatment of varied physical and neuropsychiatric disorders, especially in major depression. The intracranial electromagnetic field is generated by the the time-varying current in the stimulation coil to change the potential of targeted neurons during the treatment. Since different mental disorders correspond to specific stimulation targets and broad stimulation range might raise serious side effects, stimulation focalization is very important in TMS. To achieve focalized stimulation, a novel magnetic stimulation coil with the field shaper and crescent ferromagnetic core (the FSMC coil) is proposed and optimized in this study. The Finite-Element Method (FEM) is adopted to analyze the relationships between the design parameters of the field shaper and crescent ferromagnetic core and the characteristics of the intracranial electromagnetic field. Compared to traditional single circular coil, the focalization of the intracranial electromagnetic field generated by the optimized FSMC coil can be significantly improved both from 2D and 3D levels. To verify our method, an anatomically realistic human head model with different electrical properties assigned to each tissue of the brain is employed in this paper. We also checked the maximum induced charge density on the targeted plane generated by the optimized coil to make sure that it will not cause any induced neurologic damage.

1. INTRODUCTION

As an emerging neuromodulation method, transcranial magnetic stimulation (TMS) has been proved to be an effective tool in medical research and clinical application [1, 2]. During the treatment, TMS coil is usually placed near the human head, and the time-varying current applied in the coil generates a spatial electromagnetic field within the interested brain tissues to change the membrane potential of intracranial neurons [3, 4]. When the neuron membrane potential exceeds the excitation threshold, it will cause the depolarization of local brain nerve cells, cause excitatory action potential, and produce a series of physiological and biochemical reactions. These pulsed stimulations are known to correct the impaired functioning of cells and aid healing [5, 6]. Repetitive TMS works on similar principles and thus leads to observable clinical effects [6, 7]. The human brain structure is very complex, and the precise mechanism underlying the stimulation of neurons by the electromagnetic field is still unclear. It is generally accepted that the mechanism of transcranial magnetic stimulation is related to membrane potential, ion channel, and synaptic plasticity [5, 8–10]. To avoid unnecessary side effects caused by non-targeted brain tissues exposed to strong electromagnetic fields, it is important to limit the stimulated volume or stimulated area to a small region.

Until now, many efforts have been made on the geometric design of the TMS coil aiming to improve the spatial distributions of the intracranial induced field [11–14]. In 1985, single circular coil (SC

Received 18 June 2021, Accepted 13 September 2021, Scheduled 17 September 2021

* Corresponding author: Xiao Fang (736618304@qq.com).

¹ College of Nuclear Technology and Automation Engineering, Chengdu University of Technology, Chengdu 610059, China.

² State Key Laboratory of Advanced Electromagnetic Engineering and Technology, Huazhong University of Science and Technology, Wuhan 430074, China.

coil) was brought up along with the concept of TMS [15]. To improve the stimulation intensity and stimulation focalization, the Figure of Eight coil (FOE coil) that consists of two circular coils was proposed. The SC coil is suitable for deep brain stimulation, but the focalization of the SC coil is not as satisfied as the FOE coil [16]. In 2001, to generate a more focalized induced field, the three-dimensional (3-D) differential coil consists of two circular coils with two wing units and a bottom unit was proposed [17]. This design can improve stimulation focalization, but it will make the stimulation coil much heavier and is not friendly for doctors to move and locate. Another representative and effective design is adding a shield with a window to the coil pair. This method was proposed in 2006. It can narrow down the focusing area, but the magnetic flux density (B-field) and induced electric field (E-field) were reduced by 22.2% and 55% due to the shield [18]. In 2016, Xiong et al. designed a five-coil array to improve the stimulation focalization, and a hybrid optimization algorithm was adopted to optimize the currents applied in the coil array [19]. In 2020, Sorkhabi et al. improved the stimulation focalization with two SC coils at specific angles, and the frequencies of the currents in the two coils are different [20]. In 2021, Lindl et al. brought up the 3-axis magnetic coil to enable focusing of the induced field without any physical movement of the coils. In most of the existing designs, intracranial focalization was usually evaluated on a 2D level by the focusing area on the target plane [21]. However, since the electromagnetic fields are three-dimensional within the human head, the volume within the human brain exposed to a strong electromagnetic field should also be fully considered and analyzed.

In this study, a novel stimulation coil with the field shaper and crescent ferromagnetic core that can produce a focalized electromagnetic field within the human brain is proposed and designed. An anatomically realistic human head model is employed to verify this method. The Finite-Element Method (FEM) is adopted to analyze the spatial distributions of the electromagnetic field within the gray matter. The difference between focalization of induced B-field and the focalization of induced E-field under different coil design parameters is analyzed. Results show that the characteristics of the intracranial induced electromagnetic field generated by the proposed new magnetic coil are superior to that of traditional stimulation coil from both 2D and 3D levels.

2. METHODS

2.1. Principles of the Field Shaper

The field shaper is commonly used in the research of electromagnetic forming, and it is usually made of metal material. Because of the special geometric structure of the field shaper, the electromagnetic field generated by the time-varying current in the coil can be concentrated in a smaller area by the field shaper, thus obtaining a stronger induced field and benefiting the forming process. Inspired by the principle of its application, the field shaper can also be used in TMS to generate a focalized electromagnetic field.

The field shaper used in this paper is made of copper with a conductivity of 5.08×10^7 S/m. The 3D geometry of the field shaper is shown in Fig. 1, and the field shaper is of cone-shaped structure

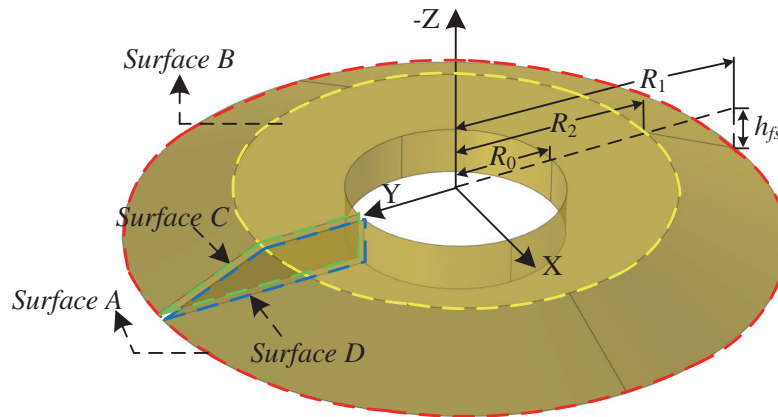


Figure 1. The 3D geometry of the field shaper.

with a central hole and a side slit. The radius of *Surface A* (marked with red dash line) and *Surface B* (marked with yellow dash line) are R_1 and R_2 , respectively. The surfaces of the side slit are indicated as *Surface C* (marked with green dash line) and *Surface D* (marked with blue dash line), respectively. The radius of the central hole is R_0 , and the thickness of the field shaper is h_{fs} . When being applied in TMS, *Surface A* with a larger radius faces the stimulation coil, and *Surface B* with a smaller radius faces the human head.

During the treatment, the exciting current flows through the stimulation coil; time-varying induced B-field is produced in the space around the coil; induced eddy current is generated in the field shaper. The flow directions of induced eddy currents on *Surface A*, *Surface B*, *Surface C*, and *Surface D* are shown in Fig. 2–Fig. 3.

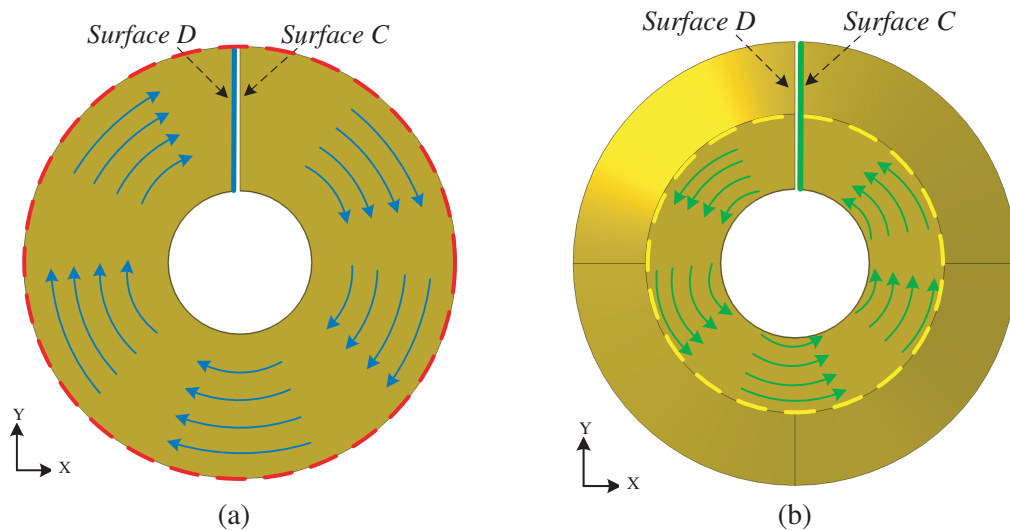


Figure 2. The induced currents on the top surface and the bottom surface of the field shaper. (a) Current direction on Surface A. (b) Current direction on Surface B.)

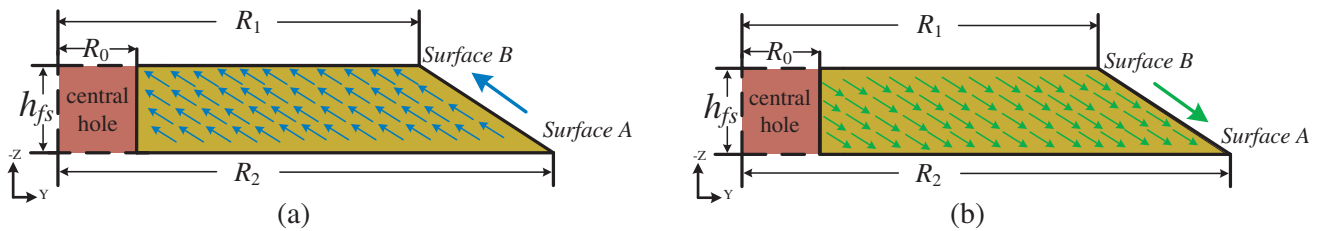


Figure 3. The induced currents on the side slit of the field shaper. (a) Current direction on Surface D. (b) Current direction on Surface C.

Assuming that the current in the stimulation coil flows counterclockwise, the induced current on *Surface A* of the field shaper will flow clockwise when being observed along the Z-axis, as shown in Fig. 2(a).

Because of the existence of the side slit, the induced eddy current on *Surface A* of the field shaper flows to *Surface B* through *Surface D* of the side slit. As shown in Fig. 3(a), the induced current on *Surface D* flows towards the central hole.

Figure 2(b) shows the flow direction of the induced current on *Surface B*. Observed along the Z-axis, the induced current flows from *Surface D* of the side slit to *Surface B* and then continues to flow in the counterclockwise direction. The current flow direction on *Surface C* of the side slit is shown in Fig. 3(b).

The induced current on *Surface B* flows back to *Surface A* through *Surface C* of the side slit. At this point, the circulating flow of the induced current in the field shaper is completed. The induced current is concentrated on *Surface B* which has a smaller area and is closer to a human head. The directions of stimulation current in the coil and the induced current on *Surface B* of the field shaper are the same.

The electromagnetic fields generated by the stimulation current and the induced eddy current are superimposed in the human head, resulting in a focused electromagnetic field in the target area, thus improving the neural regulation effect. It should be noted that the arrows in Fig. 2–Fig. 3 indicate the current flow directions, and the induced currents on these surfaces are not evenly distributed in practice.

2.2. Principle of the Crescent Ferromagnetic Core

Though the existence of field shaper is beneficial to the forming of focalized electromagnetic field, it will also weaken the intensity of the electromagnetic field. To overcome this shortcoming, the crescent ferromagnetic core is further proposed to enhance the strength of the intracranial electromagnetic field.

As shown in Fig. 4, the crescent-shaped ferromagnetic core is a part of a circular ring and is placed above the stimulation coil. The inner diameter and outer diameter of the circular ring are consistent with the stimulation coil. The spreading angle of the crescent ferromagnetic core is θ , and the thickness is h_{mc} . To avoid sharp corners, eight vertices of the ferromagnetic core are filleted with a radius of 5 mm.

The magnetic permeability of the crescent ferromagnetic core was set at 2500 which is much larger than that of the air gap. As shown in Fig. 5, the magnetic induction lines prefer to pass through the core rather than the air gap. The magnetic induction lines are concentrated around the crescent

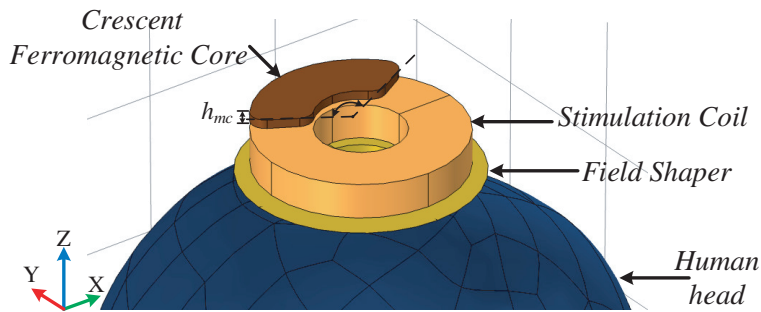


Figure 4. The 3D geometry of the field shaper.

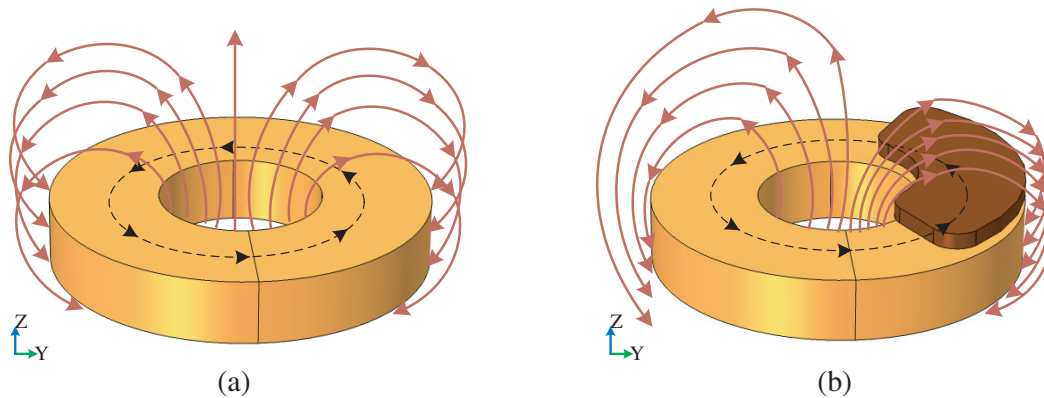


Figure 5. The magnetic induction lines on YZ plane. (a) The coil without the crescent-shaped ferromagnetic core. (b) The coil with the crescent-shaped ferromagnetic core.

ferromagnetic core so that intensity of the electromagnetic field in the intracranial target area under the crescent ferromagnetic core can be strengthened.

2.3. The 3D Model Establishment

2.3.1. Real Human Head Model

The real human head model used in this study is model numbered 101309 in the Population Head Model (PHM) Repository (<https://itis.swiss/virtual-population/regional-human-models/phm-repository/>). The PHM repository was developed by Lee et al. using the SimNIBS pipeline, which was utilized to segment anatomical regions from Human Connectome Project MRI images [22]. There are 50 unique models in the PHM repository, and these models were created from healthy young adults in the age range of 22–35 years.

The real human head model was imported to Comsol 5.2 platform, and the finite-element (FE) method was adopted to calculate the spatial distribution of the intracranial electromagnetic field. The biological conductivities of skin, skull, and gray matter are 2.01×10^{-4} S/m, 2.032×10^{-2} S/m, and 1.07×10^{-1} S/m, respectively [23]. The finalized meshed geometry of the human head model consists of 228098 domain elements, 37828 boundary elements, and 7297 edge elements.

We imported the data from the PHM repository into the Geomagic Design platform and obtain the real human head model. The 3D human head entity model and the perspective model are shown in Fig. 6.

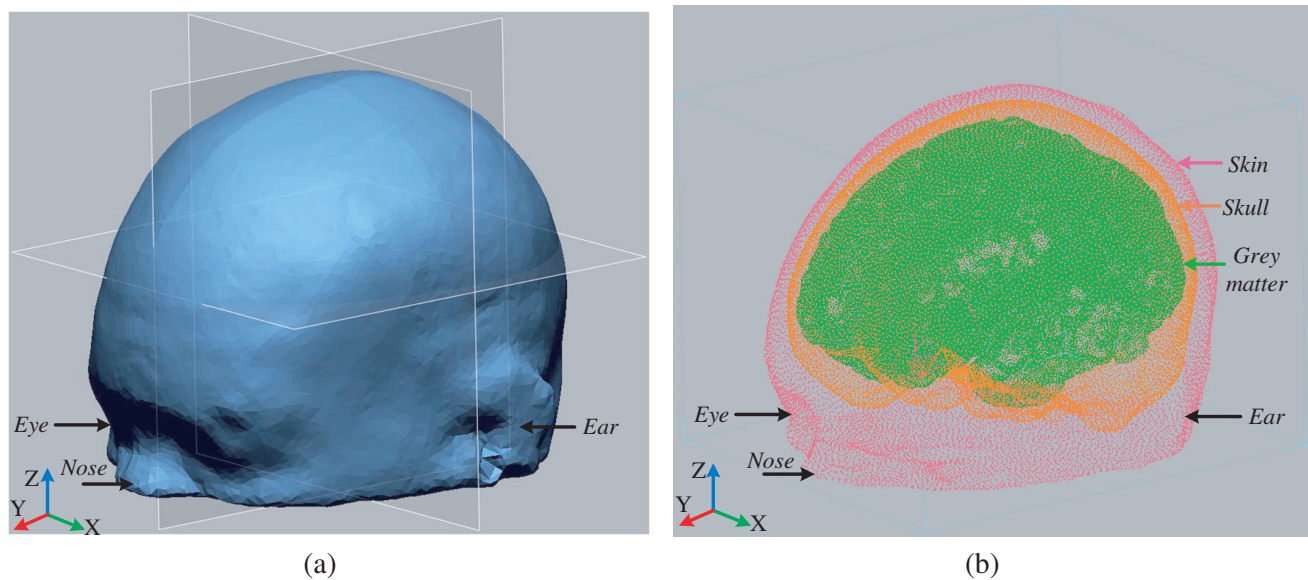


Figure 6. The 3D model of the real human head of Geomagic Designer platform. (a) The 3D human head entity model. (b) The 3D human head perspective model

The human head with a realistic structure can serve the purpose of this paper. However, if the unique responses of individuals to TMS are studied, more head models should be discussed and compared. Considering that 3-D numerical simulation takes too much calculation, it will need computers with larger memory.

2.3.2. The Stimulation Coil Model

The single circular stimulation coil (SC coil) used in this paper is wound by copper wire with a common conductivity of 5.998×10^7 S/m and a wire size of $3 \text{ mm} \times 4 \text{ mm}$. The outer radius, inner radius, and height of the coil are $r_1 = 35 \text{ mm}$, $r_2 = 15 \text{ mm}$, and $h = 12 \text{ mm}$, respectively. The amplitude of the stimulation current is 4200 A, and the width pulse is 278 μs . The repetitive frequency is set at 20 Hz.

To analyze and compare the influences of field shaper and crescent ferromagnetic core on characteristics of different coils, the SC coil is employed as a reference in this paper. The single circular stimulation coil with the field shaper is referred to as the FS coil. The single circular stimulation coil with both field shaper and ferromagnetic core is referred to as the FSMC coil. The placements of the FS coil and FSMC coil are shown in Fig. 7. The original point of the coordinate system is located at the vertex of the scalp. Considering the thickness of the coil package and the hindrance of hair in practicality, the distance between the human head and the stimulation coil is set at 8 mm.

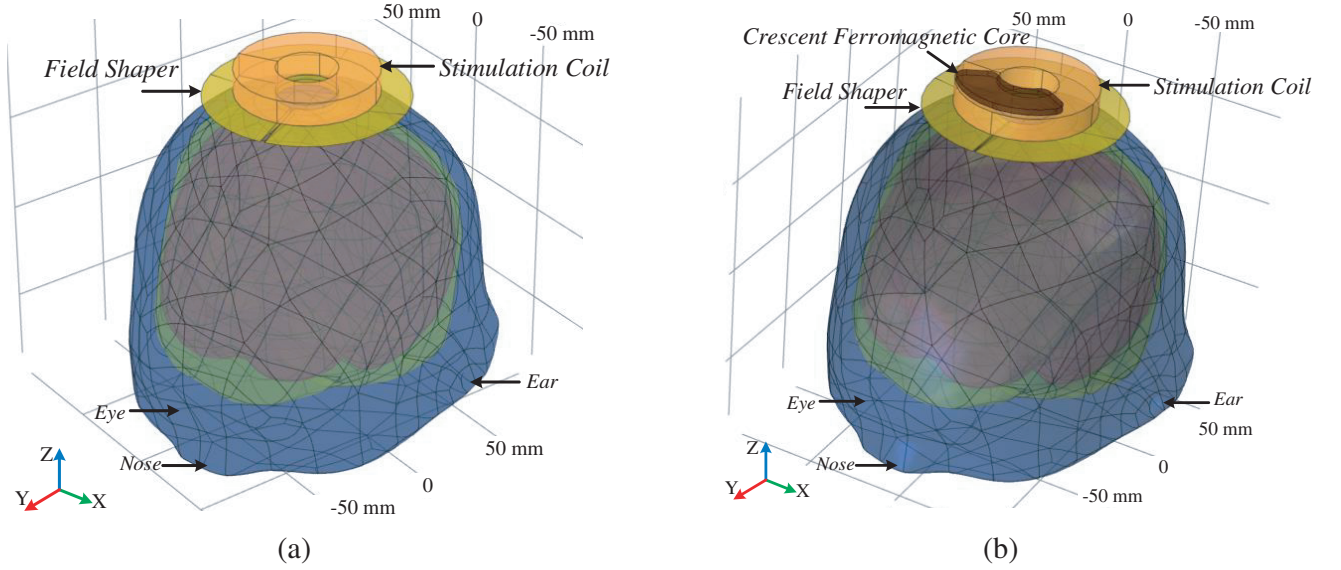


Figure 7. The placements of FS coil and FSMC coil. (a) The relative position of FS coil and the real human head. (b) The relative position of FSMS coil and the real human head.

Since the targeted tissues of many mental disorders are not superficial, the target plane is assumed to be 20 mm below the apex of the human scalp within the gray matter. Point ① and Point ② are the intersections of the *B*-field test line ($X = 0, Y = 0$), the *E*-field test line ($X = 0, Y = 25$ mm), and the target plane, respectively. The magnetic flux density B_0 is extracted at Point ①, and the intracranial the *E*-field norm E_0 is extracted at Point ②. The test lines and targeted points are shown in Fig. 8.

2.3.3. Meshes

To disregard mesh differences when comparing the electromagnetic characteristics of different coils, all FE models had the same mesh size and were computed twice. Details about the mesh size for coils are: the maximum element size is 0.050 m; the minimum element size is 0.001 m; the maximum element growth is 1.5; the curvature factor is 0.6. The level of the grid is fine enough, and the computation converges smoothly.

2.3.4. Evaluating Indicators

$V_{1/2}$ and $S_{1/2}$ are adopted in this paper to measure the 3D focalization and 2D focalization of different stimulation coils respectively [24]. $V_{1/2B}$ (cm^3), $V_{1/2E}$ (cm^3) are the volume of gray matter within which the induced *B*-field and induced electrical field exceeding half of B_0 and E_0 , respectively. $S_{1/2B}$ (cm^2), $S_{1/2E}$ (cm^2) are the area of the gray matter surface where the induced *B*-field and induced *E*-field exceeding half of B_0 and E_0 , respectively.

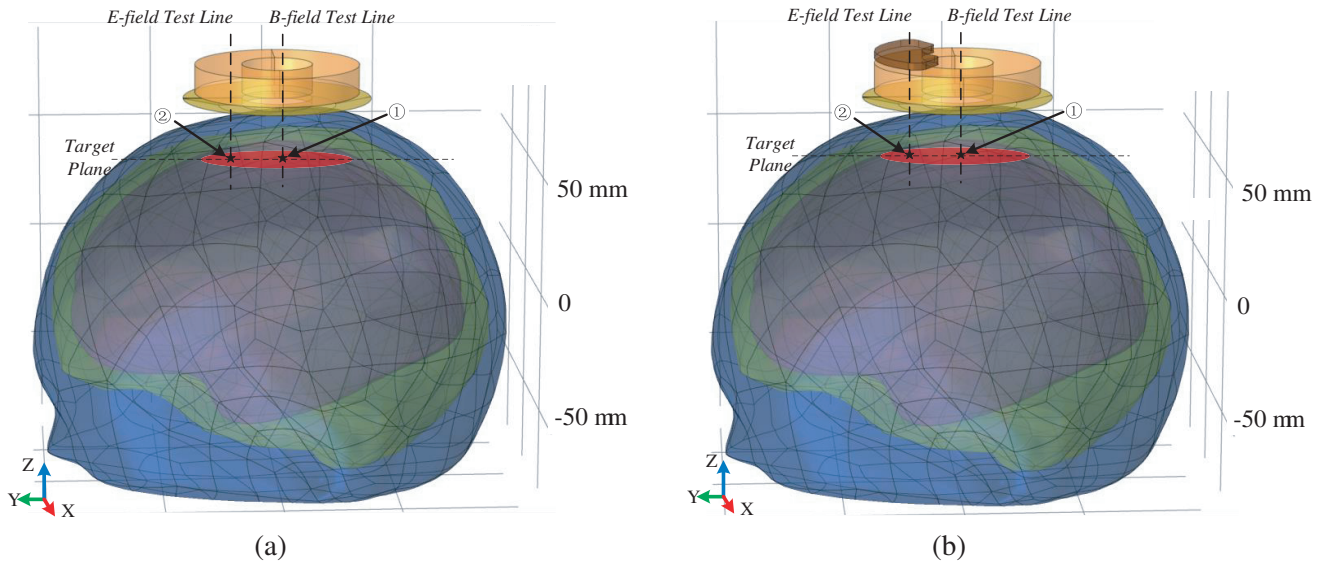


Figure 8. The test lines and targeted points. (a) The test lines and targeted points when the FS coil is placed above human head. (b) The test lines and targeted points when the FSMC coil is placed above human head.

3. RESULTS AND ANALYSIS

3.1. Relationships between Field Shaper Design Parameters and the Characteristics of Intracranial Electromagnetic Field

Aiming to find out the influence of field shaper on coil electromagnetic characteristics, multiple FS coils were modeled with varied field shaper design parameters.

The FS coils were divided into three experimental groups to show the effects of R_1/R_2 , R_0 , and h_{fs} .

3.1.1. Effect of R_1/R_2

The ratio of R_1/R_2 which is referred as the relative radius of the field shaper reflects the asymmetry of *Surface A* and *Surface B*. Keeping the radius of *Surface B* at $R_2 = 25$ mm and increasing the value of R_1 , we can obtain five different FS coils with different R_1/R_2 .

As shown in Fig. 9(a), for both B-field and E-field, with the increase of R_1/R_2 , the focalizing volume and focalizing area within the gray matter are firstly decreased and then increased.

Considering the change degree of $V_{1/2}$ and $S_{1/2}$, the difference between the maximum variation ratio of the B-field and the E-field is not obvious (as the blue text and red text marked in Fig. 9(a)). $V_{1/2B}$, $V_{1/2E}$, $S_{1/2B}$, and $S_{1/2E}$ reach their lowest values when R_1/R_2 is between 1.8 and 2. It proves that there is an optimum ratio of R_1/R_2 that benefits focalization most. The reason is that with the increase of R_1/R_2 , the asymmetry of *Surface A* and *Surface B* becomes more prominent, and the electromagnetic energy generated by the coil is concentrated in a smaller area so that the focalization is improved. However, with a further increase of R_1/R_2 , the size of the *Surface A* is too large; energy loss is intensified; the stimulation focalization induced is weakened.

3.1.2. Effect of R_0

The R_0 experimental group is constructed by maintaining $R_1/R_2 = 1.6$, $h_{fs} = 3$ mm, while ranging the central hole radius of the field shaper from $R_0 = 15$ mm to $R_0 = 35$ mm. As shown in Fig. 9(b), the focusing volume and focusing area show a declining trend after an initial ascent. Observing from the maximum variation ratio, the focalization of induced B-field is more sensitive to the change of R_0

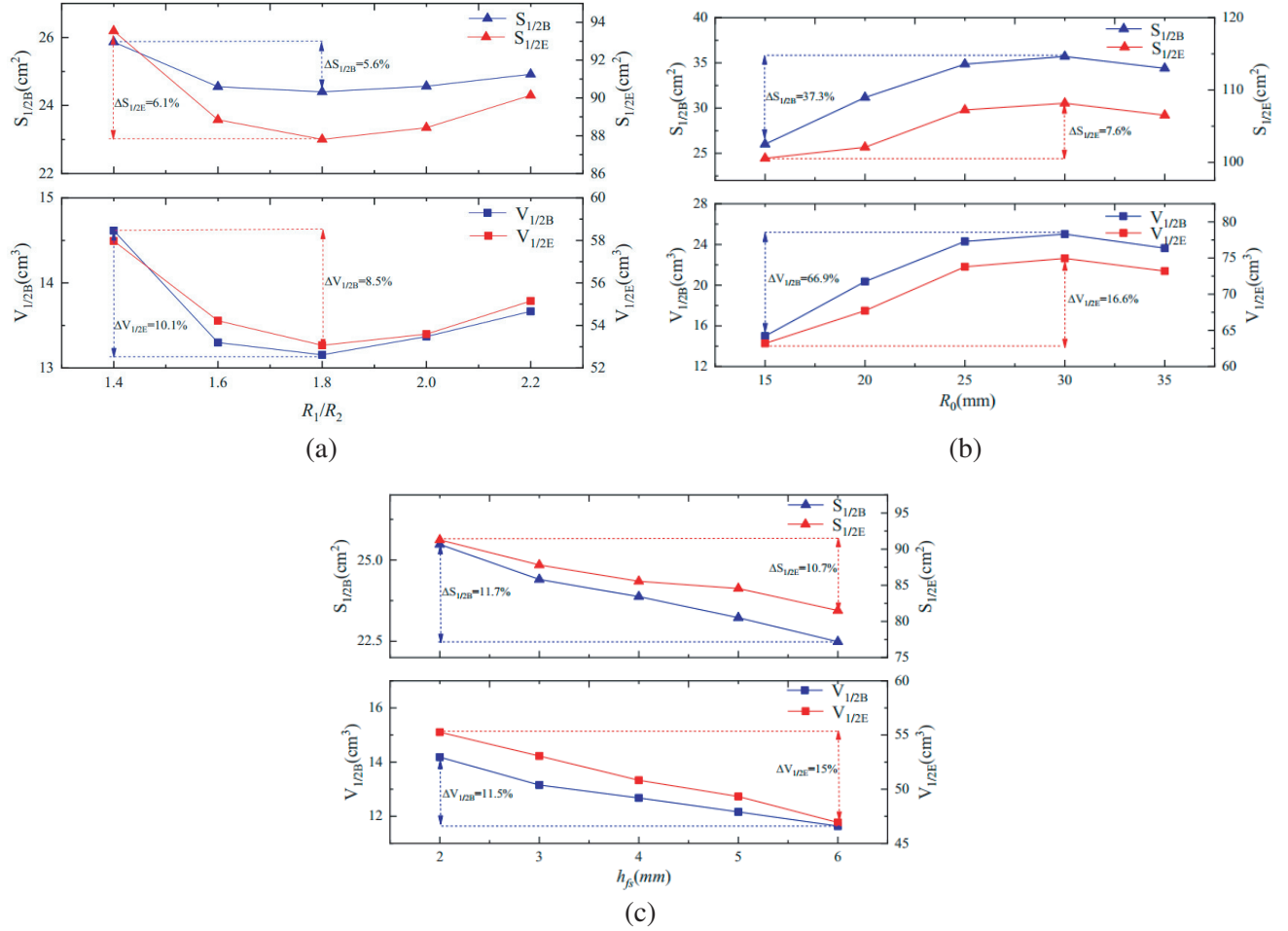


Figure 9. Relationships between field shaper design parameters and the characteristics of intracranial electromagnetic field. (a) Influences of R_1/R_2 on $V_{1/2B}$, $V_{1/2E}$, $S_{1/2B}$ and $S_{1/2E}$. (b) Influences of R_0 on $V_{1/2B}$, $V_{1/2E}$, $S_{1/2B}$ and $S_{1/2E}$. (c) Influences of h_{fs} on $V_{1/2B}$, $V_{1/2E}$, $S_{1/2B}$ and $S_{1/2E}$.

than the E-field. With the increase of R_0 , more magnetic induction lines go through the central hole into the human head without passing the field shaper, thus more unexpected tissues are exposed in the electromagnetic field, and the focalization is weakened. When R_0 reaches the inner radius of the coil which is $r_1 = 35$ mm, a strong induced B-field generated in the center of the coil is not received by the field shaper, and the field shaper's effect is similar to a shield plate, so the focus of the intracranial electromagnetic field is improved compared to $R_0 = 30$ mm, but at the same time, the peak value of the intracranial electromagnetic field is reduced.

3.1.3. Effect of h_{fs}

As shown in Fig. 9(c), the intracranial focalization is improved with the increase of h_{fs} , and the improvement between $h_{fs} = 2$ and $h_{fs} = 3$ is more obvious. This phenomenon can be explained as follows: The induced currents on *Surface A* and *Surface B* of field shaper are equal in magnitude and opposite in direction. The skin depths of *Surface A* and *Surface B* are the same, when h_{fs} is less than the sum of the skin depths of the two surfaces. Induced currents on *Surface A* and *Surface B* will be counteracted, and the effect of the field shaper is weakened. When the stimulation current frequency $f = 3600$ Hz, the skin depth δ of the field shaper is about 2×1.1 mm, so that when $h_{fs} = 2$ mm $<$ 2.2 mm, the field shaper does not serve the purpose of improving focalization, and when h_{fs} increases from 2 mm to 3 mm, both $V_{1/2}$ and $S_{1/2}$ are improved. Also, the maximum variation ratios of $S_{1/2}$ for B-field and

E-field are similar, and the maximum variation ratio of $V_{1/2}$ for the E-field is slightly larger than that of B-field, which means that with the change of h_{fs} , $V_{1/2E}$ is more affected than $V_{1/2B}$.

3.2. Relationship between Ferromagnetic Core Design Parameters and Coil Electromagnetic Characteristics

To further improve the focalization, multiple FSMC coils were modeled with different ferromagnetic cores. The geometric parameters of the field shaper in these FSMC coils are constant with $R_1 = 45$ mm, $R_2 = 25$ mm, $R_0 = 15$ mm, and $h_{fs} = 3$ mm. The FSMC coils were divided into two experimental groups to show the effects of θ and h_{mc} .

3.2.1. Effect of θ

The θ experiment group is constructed by keeping the $h_{mc} = 3$ mm and ranging the spreading angle from $\theta = 60^\circ$ to $\theta = 180^\circ$ at the step of 30° . As shown in Fig. 10(a), for B-field, the stimulation focalization ($V_{1/2}$, $V_{1/2}$) and stimulation intensity (the magnitude of B-field) within the gray matter is not sensitive to the changes of θ . From Fig. 10(a), we can see that, for the E-field, with the increase of spreading angle θ , both $V_{1/2}$ and $S_{1/2}$ decrease firstly and then have a slight increase. $\theta = 150^\circ$ is an optimum spreading angle considering $V_{1/2E}$ and $S_{1/2E}$. Fig. 10(a) shows that the induced E-field strength is slightly improved with the increase of θ .

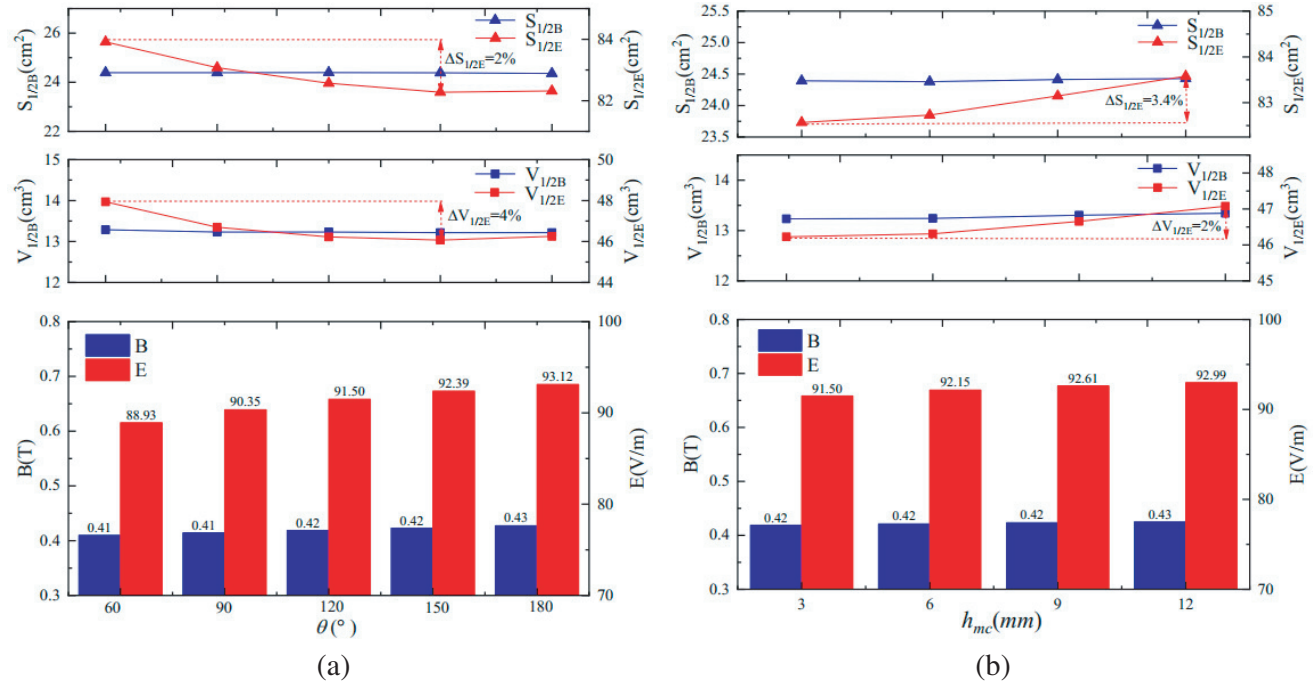


Figure 10. Relationships between the crescent ferromagnetic core design parameters and the characteristics of intracranial electromagnetic field. (a) Influences of θ on electromagnetic field. (b) Influences of h_{mc} on electromagnetic field.

3.2.2. Effect of h_{mc}

The h_{mc} experiment group is constructed by keeping the $\theta = 120^\circ$ and ranging the thickness of the ferromagnetic core from $h_{mc} = 3$ mm to $h_{mc} = 12$ mm at the step of 3 mm. From Fig. 10(b), it can be seen that the B-field remains insensitive to the changes of h_{mc} . For E-field, the intracranial focalization is gradually weakened with the increase of h_{mc} , while the intensity of E-field is slightly improved. Considering the E-field, the optimized h_{mc} should not be too large nor too small.

3.3. Comparisons among SC Coil, FS Coil, and FSMC Coil

To enable meaningful comparison, the optimized FS coil and optimized FSMC coil are constructed based on the analysis in *Section A* and *Section B*. Geometric parameters for the optimized FS coil are set at $R_1/R_2 = 1.8$, $R_0 = 15$ mm, and $h_{fs} = 6$ mm. Geometric parameters for the optimized FSMC coil are set at $\theta = 150^\circ$, $h_{mc} = 9$ mm. Figs. 11(a), (b), (c) show the magnetic flux densities on the YZ plane generated by the SC coil, optimized FS coil, and optimized FSMC coil, respectively.

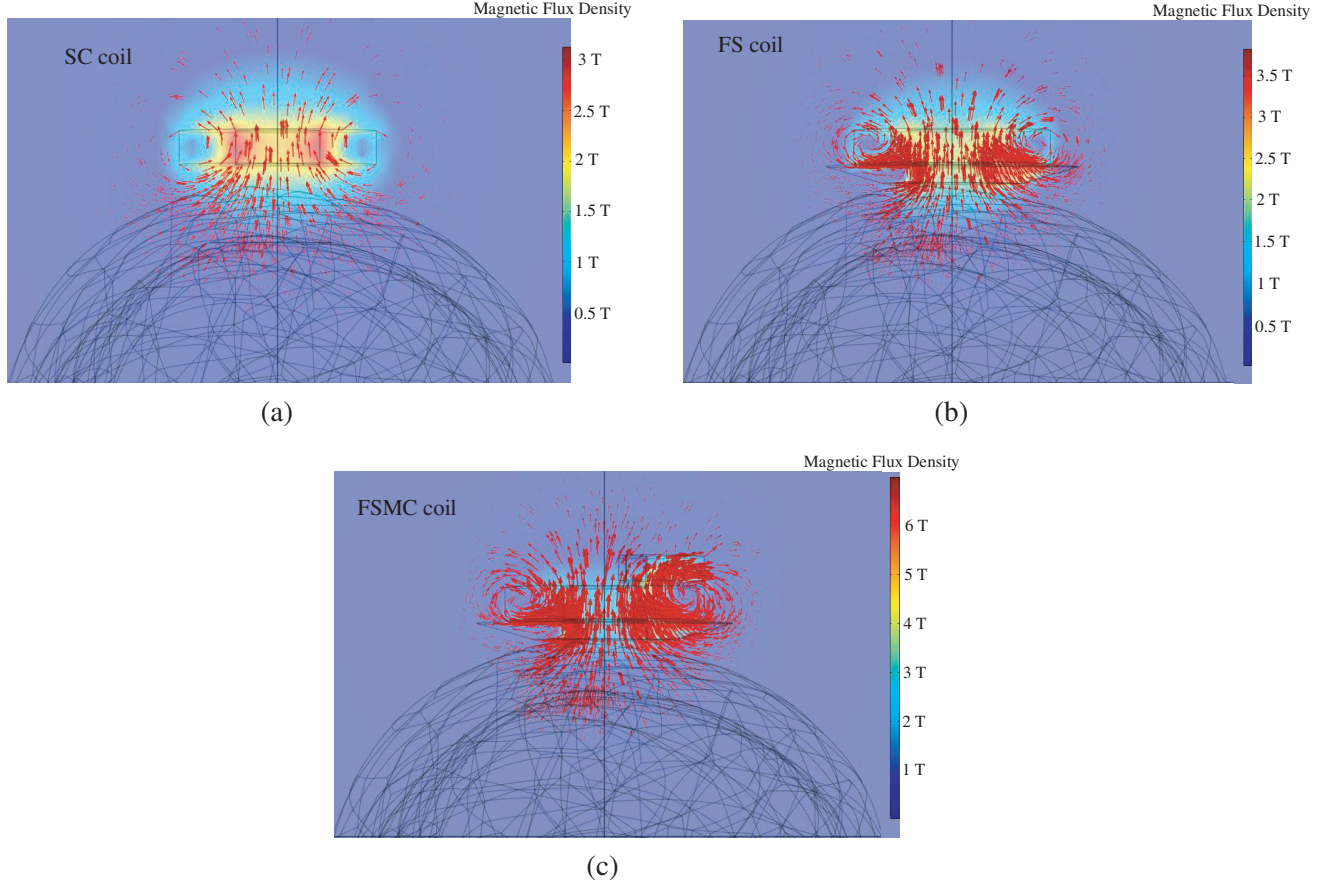


Figure 11. The magnetic flux density on YZ plane generated by different coils. (a) The magnetic flux density generated by the SC coil. (b) The magnetic flux density generated by the optimized FS coil. (c) The magnetic flux density generated by the optimized FSMC coil

As we can see from Fig. 11, the existence of the field shaper is beneficial to the forming of a focused induced B-field, and the ferromagnetic core can significantly improve the peak value of the induced B-field.

Characteristics of the intracranial electromagnetic field generated by the SC Coil, optimized FS Coil, and optimized FSMC Coil are presented in Table 1. As in Table 1, the field shaper is capable of improving the focalization characteristics of the stimulation coil from both 2D and 3D levels.

However, the presence of a field shaper will also weaken the intensity of the intracranial electromagnetic field. Although the percentage of the decrease is not as bad as the previously proposed shielding plate with window (about 55%) [18], the field shaper still weakens the intensity of the induced E-field by 12.2%. The crescent ferromagnetic core just makes up for this shortcoming: When the core is added, the strength of the induced B-field is enhanced by 7%, and the decrease percentage of the induced electrical field intensity is reduced to 3%.

The optimized FSMC coil can improve the 2D focalization and 3D focalization of the intracranial

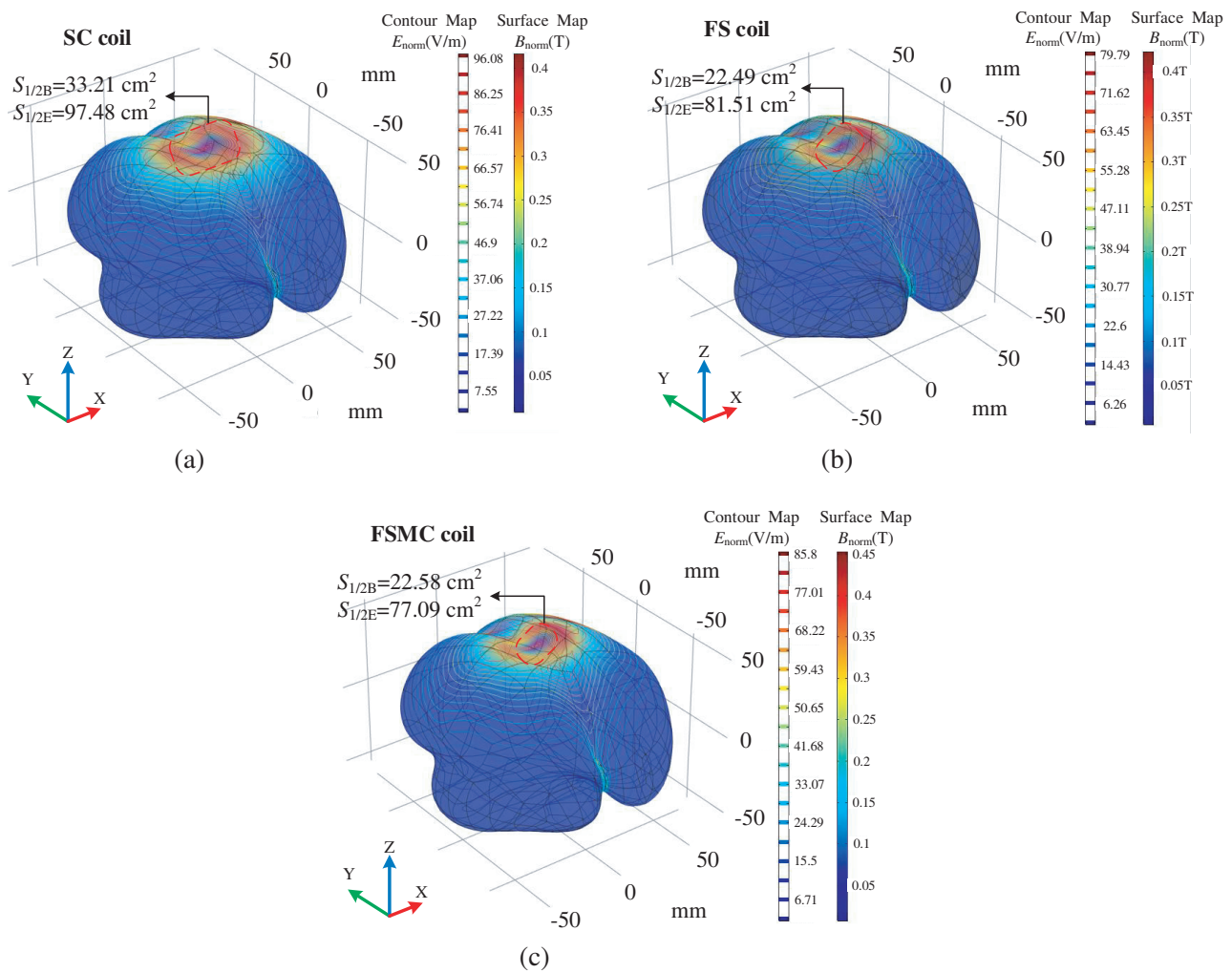


Figure 12. Comparison of the electromagnetic field distributions within gray matter generated by different coils. (a) The electromagnetic fields generated by the SC coil. (b) The electromagnetic fields generated by the optimized FS coil. (c) The electromagnetic fields generated by the optimized FSMC coil.

Table 1. Electromagnetic characteristics of different coils.

	SC coil	Optimized FS coil	Optimized FSMC coil	Improvement
B_0 (T)	0.43	0.43	0.46	+7%
E_0 (V/m)	99.6	87.44	96.37	-3%
$V_{1/2B}$ (cm^3)	21.77	11.69	11.57	+47%
$V_{1/2E}$ (cm^3)	67.73	46.91	41.35	+39%
$S_{1/2B}$ (cm^2)	33.21	22.49	22.58	+32%
$S_{1/2E}$ (cm^2)	97.48	81.51	77.09	+21%

induced B-field by 32% and 47%, respectively. The optimized FSMC coil can also improve the 2D focalization and 3D focalization of the intracranial induced E-field by 21% and 39%, respectively.

The electromagnetic fields generated by the SC coil, optimized FS coil, and optimized FSMC coil are shown in Fig. 12. As we can see in Fig. 12, the electromagnetic fields produced by the optimized

FSMC coil are more focalized.

After satisfying the therapeutic demands for stimulation focalization, the induced neurologic damage which may be caused during a typical treatment is calculated. The maximum induced charge density on the targeted plane generated by the optimized FSMC coil is turned out to be $0.16 \mu\text{C}/\text{cm}^2$ per pulse which is way below the safety limit of $40 \mu\text{C}/\text{cm}^2$ per pulse [25].

It should be noted that the pulsed current in TMS usually has a high amplitude to generate sufficient induced electric field strength in the brain. When additional conductive and ferromagnetic materials are introduced, and the magnetic stimulator may generate a lot of heat after working for a long time. Therefore, in practical engineering applications, the design of the field shaper and ferromagnetic core should not only consider the focalization of induced E-field but also take the energy loss and heating problem into account, to avoid potential safety hazards caused by overheating [26, 27].

4. CONCLUSION

TMS is an effective tool in scientific research and medical treatment. In this paper, a novel TMS coil with a field shaper and crescent ferromagnetic core is proposed to narrow down the focusing area and focusing volume within the human brain. The analysis of the relationships between the design parameters of field shaper and crescent ferromagnetic core and the electromagnetic characteristics of the proposed stimulation coil shows that the sensitivities of the focalization of induced B-field and E-field to the design parameters are different.

Results prove that with the utilization of a well-designed field shaper and crescent ferromagnetic core, focalization characteristics of the TMS coil can be significantly improved from both 2D and 3D levels without greatly weakening the stimulation intensity and causing induced neurologic damage. Under the same stimulation current, the optimized FSMC coil can improve the 2D focalization and 3D focalization of the intracranial induced B-field by 32% and 47%, respectively. The optimized FSMC coil can also improve the 2D focalization and 3D focalization of the intracranial induced E-field by 21% and 39%, respectively. The maximum induced charge density on the targeted plane generated by the optimized FSMC coil is checked to be within the safety limit.

The specific design method of the field shaper and ferromagnetic core is also applicable to other stimulation coils which may bring more possibilities for the applications of TMS.

REFERENCES

1. Hand, B. J., G. M. Opie, S. K. Sidhu, et al., "TMS coil orientation and muscle activation influence lower limb intracortical excitability," *Brain Research*, Vol. 1746, 147027, 2020.
2. Sanchez, C. C., M. R. Cabello, A. Q. Olozabal, et al., Design of TMS coils with reduced Lorentz forces: Application to concurrent TMS-fMRI," *Journal of Neural Engineering*, Vol. 17, No. 1, 016056.1–016056.11, 2020.
3. Peterchev, A. V., T. A. Wagner, P. C. Miranda, et al., "Fundamentals of transcranial electric and magnetic stimulation dose: Definition, selection, and reporting practices," *Brain Stimulation*, Vol. 5, No. 4, 435–453, 2012.
4. Yi, G., J. Wang, X. Wei, et al., "Dynamic analysis of Hodgkin's three classes of neurons exposed to extremely low-frequency sinusoidal induced E-field," *Applied Mathematics & Computation*, Vol. 231, 100–110, 2014.
5. Dou, Z. and J. Liao, *Transcranial Magnetic Stimulation Technique Fundamental Theory and Clinical Practice*, People's Health Publishing House, 2012.
6. Chail, A., R. K. Saini, P. S. Bhat, et al., "Transcranial magnetic stimulation: A review of its evolution and current applications," *Industrial Psychiatry Journal*, Vol. 27, No. 2, 2018.
7. Gordon, S. R., M. Jamie, M. John, et al., "Evaluation of pulsed electromagnetic field therapy for the treatment of chronic postoperative pain following lumbar surgery: A pilot, double-blind, randomized, sham-controlled clinical trial," *Journal of Pain Research*, Vol. 11, 1209, 2018.
8. Tang, A., W. Bennett, A. Bindoff, et al., "Low intensity repetitive transcranial magnetic stimulation drives structural synaptic plasticity in the young and aged motor cortex," 2021.

9. Huang, H., "Magnetic stimulation of neurons and study of membrane structures," State University of New York at Buffalo, 2013.
10. Pfeiffer, F. and A. Benali, "Could non-invasive brain-stimulation prevent neuronal degeneration upon ion channel re-distribution and ion accumulation after demyelination?," *Neural Regeneration Research*, Vol. 15, No. 11, 1977–1980, 2020.
11. Kato, T., M. Sekino, T. Matsuzaki, et al., "Electromagnetic characteristics of eccentric figure-eight coils for transcranial magnetic stimulation: A numerical study," *Journal of Applied Physics*, Vol. 111, No. 7, Pt. 2, 22–1988, 2012.
12. Meng, Y., R. L. Hadimani, L. J. Crowther, et al., "Deep brain transcranial magnetic stimulation using variable "Halo coil" system," *Journal of Applied Physics*, Vol. 117, No. 17, 1106–128, 2015.
13. Guadagnin, V., M Parazzini, S. Fiocchi, et al., "Deep transcranial magnetic stimulation: Modeling of different coil configurations," *IEEE Transactions on Biomedical Engineering*, Vol. 63, No. 7, 1543–1550, 2016.
14. Lu, M. and S. Ueno, "Calculating the E-field in real human head by transcranial magnetic stimulation with shield plate," *Journal of Applied Physics*, Vol. 105, No. 7, 527, 2009.
15. Barker, A. T., R. I. Jalinous, and I. L. Freeston, "Non-invasive magnetic stimulation of human motor cortex," *Lancet*, Vol. 325, No. 8437, 1106–1107, 1985.
16. Yang, S., G. Xu, et al., "Circular coil array model for transcranial magnetic stimulation," *IEEE Transactions on Applied Superconductivity*, Vol. 20, 829–833, 2010.
17. Hsu, K.-H. and D. M. Durand, "A 3-D differential coil design for localized magnetic stimulation," *IEEE Transactions on Biomedical Engineering*, Vol. 48, No. 10, 1162–1168, 2001.
18. Kim, D. H., G. E. Georghiou, and C. Won, "Improved field localization in transcranial magnetic stimulation of the brain with the utilization of a conductive shield plate in the stimulator," *IEEE Transactions on Biomedical Engineering*, Vol. 53, No. 4, 720–725, 2006.
19. Xiong, H., J. H. Shi, X.-W. Hu, and J.-Z. Liu, "The focusing optimization of transcranial magnetic stimulation system," *Progress In Electromagnetics Research M*, Vol. 48, 145–154, 2016.
20. Sorkhabi, M. M., K. Wendt, and T. Denison, "Temporally interfering TMS: Focal and dynamic stimulation location," *2020 42nd Annual International Conference of the IEEE Engineering in Medicine and Biology Society (EMBC) in Conjunction with the 43rd Annual Conference of the Canadian Medical and Biological Engineering Society*, IEEE, 2020.
21. Lindl, A., A. Md, B. Am, et al. "A 3-axis coil design for multichannel TMS arrays," *Neuro Image*, 224, 2020.
22. Lee, E. G., W. Duffy, R. L. Hadimani, et al., "Investigational effect of brain-scalp distance on the efficacy of transcranial magnetic stimulation treatment in depression," *IEEE Transactions on Magnetics*, Vol. 52, No. 7, 1–4, 2016.
23. Chiu, T.-J., H.-I Lu, C.-H. Chen, et al. "Osteopontin expression is associated with the poor prognosis in patients with locally advanced esophageal squamous cell carcinoma receiving preoperative chemoradiotherapy," *BioMed Research International*, Vol. 2018, 1–9, 2018.
24. Deng, Z. D., S. H. Lisanby, A. V. Peterchev, "E-field depth-focality tradeoff in transcranial magnetic stimulation: Simulation comparison of 50 coil designs," *Brain Stimulation*, Vol. 6, No. 1, 1–13, 2013.
25. Roth, B. J., A. Pascualleone, L. G. Cohen, et al., "The heating of metal electrodes during rapid-rate magnetic stimulation: A possible safety hazard," *Electroencephalography & Clinical Neurophysiology*, Vol. 85, No. 2, 116–123, 1992.
26. Liu, C., H. Ding, X. Fang, et al., "Optimal design of transcranial magnetic stimulation thin core coil with trade-off between stimulation effect and heat energy," *IEEE Transactions on Applied Superconductivity*, Vol. 30, No. 4, 2020.
27. Saxby, P., et al., "A water-cooled transcranial magnetic stimulation coil," *Brain Stimulation*, 2008.